Nanoscale

Accepted Manuscript

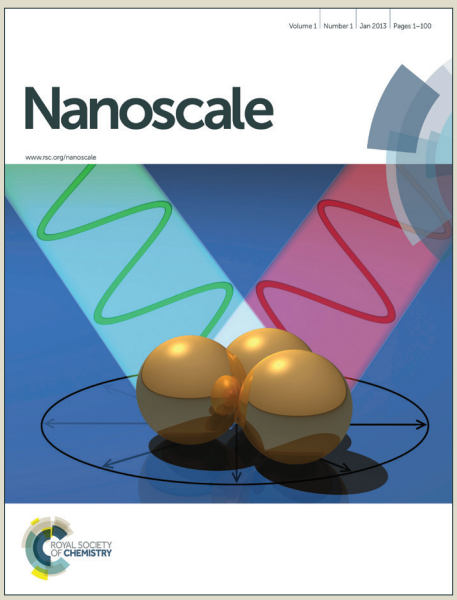

ROYAL SOCIETY OF CHEMISTRY

www.rsc.org/nanoscale

Nanoscale

RSCPublishing

FEATURE ARTICLE

Metal Non-Oxide Nanostructures Developed from Organic-Inorganic Hybrids and Their Catalytic Application

Qingsheng Gao,*[a] Ning Liu,[a] Sinong Wang,[b] and Yi Tang*[b]

Cite this: DOI: 10.1039/xoxxoooooox

Received ooth January 2012,
Accepted ooth January 2012

DOI: 10.1039/xoxxoooooox

www.rsc.org/

The rational design of metal non-oxides is important for their catalytic application, which is however limited by the current synthetic strategies being short of effective control over formation reactions. Recently, the hybrids evenly integrating organic with inorganic molecules on nanoscale significantly provide quasi-homogenous reactions towards well-defined nanocatalysts of metal non-oxides, in which their structures and properties can be modulated in a wide range. Focusing on the nanostructures and the related catalytic behaviors, this feature article seeks to provide some control on the key structures and properties of metal non-oxides (e.g., carbides, nitrides, sulfides and selenides). It is thus anticipated to shed some light on the development of emerging materials for efficient catalysis, especially those used in energy utilization.

I. Introduction

Metal non-oxides, including carbides, nitrides, sulfides *etc*., are a class of important functional materials with applications in catalysis, refractory ceramics, sensing technology, electrochemistry and optoelectronics.[1-3] Compared with relative oxides, metal non-oxides are significant for the abundant physicochemical properties associated with their electron-rich bonds and tunable interactions between metals and non-oxygen elements.[4-6] Commonly, the lower electronegativity of non-oxygen elements (*vs.* O) extends the functionalities of metal oxides. If oxides are insulators, the corresponding metal non-oxides can be semiconductors, and even in some cases, metallic properties are found.[7] Among them, the carbides and nitrides of early-transition-metals (e.g., Mo and W) often exhibit noble-metal-like catalytic properties.[1,2,8] In such compounds, the formation of alloy phases involving metal with carbon or nitrogen atoms usually enlarges the spacing of metal-metal (M-M, Scheme 1). As a result, the density of unoccupied d-orbitals is obviously reduced due to the band contraction, which leads to the DOS (density of states) around Fermi level and consequent catalytic properties similar to those of noble metals.[9] Their high performance has been well proved in hydrogenation and dehydrogenation reactions,[10,11] and the outstanding tolerance to S and CO further promotes them as the efficient and economic substitutes for high-cost precious-metal catalysts.[12,13] On the other hand, electron transfer from metals to non-oxygen elements will increase the DOS of unoccupied d-orbital, in contrast to the effect of M-M expanding owing to alloying.[14] Inspired by such two opposite mechanisms, the well-tailored electronic and surface properties are expected to be achieved via the precise control on composition and structure. As illustrated in ammonia catalytic decomposition, the introduction of N into Mo_2C obviously improved H_2 formation rate, comparable to that over Ru-based catalysts, because of the highly energetic sites involving twin boundaries, stacking faults,

Qingsheng Gao is a professor of chemistry in Jinan University, Guangzhou, China. He received his BSc degree in 2005 and PhD degree in 2010 from Fudan University, under the supervision of Prof. Yi Tang. And then, he carried out his postdoctoral research in Max-Planck Institute for Colloids and Interfaces in Germany, with Prof. Markus Antonietti and Dr. Cristina Giordano. His current research interests focus on the nanostructures of organic-inorganic hybrids and metal non-oxides, and their catalytic application for energy utilization.

Yi Tang is a professor of chemistry in Fudan University, Shanghai, China. He received his BSc degree of chemistry in 1985 and his PhD degree of physical chemistry in 1990 from Fudan University, under the supervision of Prof. Zi Gao. His research interests have been with zeolite synthesis, characterization, modification and application in catalysis and biology. He is now mainly working in the fields of synthesis, assembly and functionalization of nanozeolite as well as metal non-oxide nanocatalysts.

and defects.[15] Undoubtedly, metal non-oxides are promising catalysts for the catalytic processes during energy utilization, which usually demand high-performed materials with tunable structures, prominent properties and economic cost.

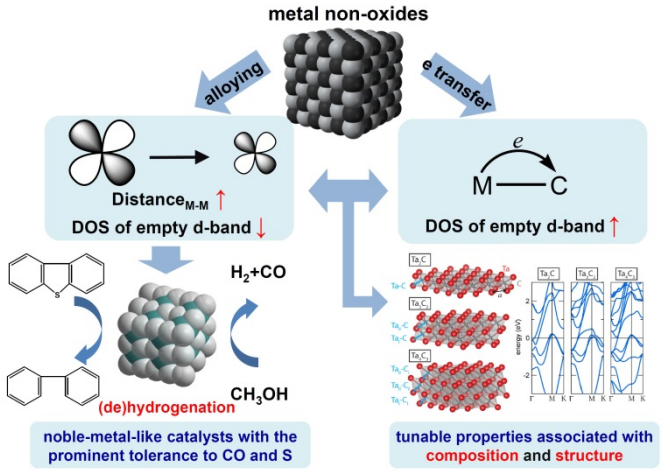

Scheme 1. Schematic illustration for the noble-metal-like catalytic properties of metal non-oxides depending on their composition and structure. Panels are reproduced with permission.[16] Copyrights IOP Publishing (2013)

Most of metal non-oxides are traditionally prepared via temperature programmed reduction (TPRe) methods employing the gas-solid reactions between relative oxides with carbon/nitrogen/sulfur-containing gases (e.g., CH_4/H_2, NH_3 and H_2S).[17-19] Such flows are flammable, corrosive or environment-unfriendly. Incomplete transformation is difficult to avoid since the reactions take place only on gas-solid interfaces, inducing the obvious difference between surface and bulk-phase. In particular, the polymeric carbon species on metal carbides resulting from the pyrolysis of excessive carbon-containing gases would cover the active sites of products and unfortunately reduce the catalytic activity.[20] Meanwhile, the composition and crystallographic structure essentially deciding the catalytic behaviors of metal non-oxides are not easy to control due to the overreactions during high-temperature treatment, especially in the case of gas-solid interface reactions. For example, TaON and Ta_3N_5, the novel visible-light-driven photocatalysts, usually suffer the over-nitridation to inactive Ta_4N_5 and TaN by-products.[18] Additionally, the complex and strict synthetic conditions, such as harsh control on temperature ramping rate, gas components, and flow rate, inhibit the scaled preparation and further application.[17,18] Thus, new and facile synthetic strategies with the precise modulation over catalyst structure and property are highly demanded.

Organic-inorganic hybrid materials integrating two counterparts into a single structure on nanoscale have recently provided special opportunities towards functional nanostructures of metal non-oxides. Noticeably, the presence of inorganic framework in sub-nanometer dimension surrounded by active organic molecules (containing C, N or S) can facilitate the quasi-homogeneous generation of metal non-oxides, avoiding the use of flammable, corrosive and environment-unfriendly flows, e.g., H_2, NH_3 and H_2S. Such innovation significantly expresses the unique merits for catalyst design. Firstly, the quasi-homogeneous generation of metal non-oxides evolved from the body of organic-inorganic nanohybrids successfully avoids the disadvantages of gas-solid reactions in TPRe, ensuring the easy manipulation, complete reactions, and nanosized products with well-defined structures.[20,21] Secondly, effective control over the transformation of organic and inorganic counterparts can be introduced into reactions to further tailor the composition, crystallographic structure, surface property of non-oxides.[22,23] Thirdly, the synchronous evolutions of precursor topologic-deformation and non-oxide generation benefit the versatile fabrication of hierarchical nanocatalysts, synergistically enhancing the features of various building blocks with multi-dimensions and multi-phases.[24,25]

Recently, significant progresses have been made in developing nanosized metal non-oxides via the controlled evolution of organic-inorganic hybrids, and exploring the catalytic applications to optimize the efficiency, processability, stability, and cost-effectiveness. Regarding the rapidly booming attention in this cutting-edge area, it is necessary to highlight the new discoveries and achievements in the past few years. In this feature article, special focus is put on several non-oxide nanostructures of transition-metal (e.g., Mo, W, Ta, Fe and Co) with prominent catalytic applications.

II. Metal carbides

Transition-metal carbides, e.g., Mo_2C, WC, W_2C and Fe_3C, have been used as efficient catalysts for hydrogenation and dehydrogenation processes due to their noble-metal-like catalytic properties.[2] As mentioned above, incomplete conversion and surface carbon-deposition are difficult to avoid owing to the gas-solid interface reactions in conventional TPRe methods.[20] Other routes of chemical vapor deposition,[26] sonochemistry[27] and $NaBEt_3H$-reduction[28] also suffer the complex associated with harsh manipulation. In the recent work,[20,21,29,30] organic-inorganic nanohybrids were introduced to fabricate nanosized carbides via quasi-homogeneous reactions between sub-nanometer-contacting inorganic (metal source) and organic molecules (carbon source). This successfully avoids the disadvantages of interface reactions in TPRe and other methods.

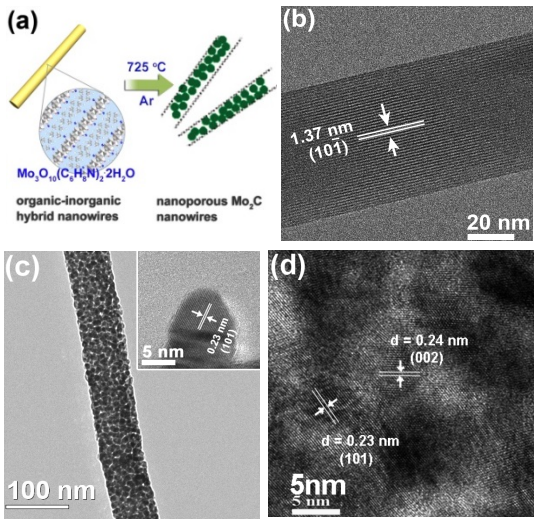

Fig. 1 (a) Schematic illustration for synthesis of Mo_2C-based nanocatalyst from $Mo_3O_{10}(C_6H_5NH_3)_2{\cdot}2H_2O$ nanowires. TEM images of (b) $Mo_3O_{10}(C_6H_5NH_3)_2{\cdot}2H_2O$ nanowires, (c, d) nanoporous Mo_2C nanowires. Panels are reproduced with permission.[21,31] Copyrights ACS (2009) and RSC (2014).

Taking Mo_2C as an example, its facile synthesis has been achieved based on MoO_x/amine precursors (Fig. 1a).[21] The hybrid structure of $Mo_3O_{10}(C_6H_5NH_3)_2{\cdot}2H_2O$ nanowires (Fig. 1b) benefited the generation of one-dimensional (1D) Mo_2C composed of small nanoparticles via easy calcination under inert flow (Fig. 1c and 1d). The uniform reactions throughout precursors, employing aniline as both reducing agent and carbon source, significantly promoted the preparation to several grammes, dozens of times of the limitation in typical TPRe. The abundant nanoporosity and large surface (51 ~ 65 m^2/g) free from depositing carbon (Fig. 1c) suggest the good surface activity of Mo_2C. In the production of H_2 from methanol catalytic decomposition, Mo_2C nanowires delivered the obviously enhanced activity and stability in comparison with Mo_2C derived from TPRe.[21]

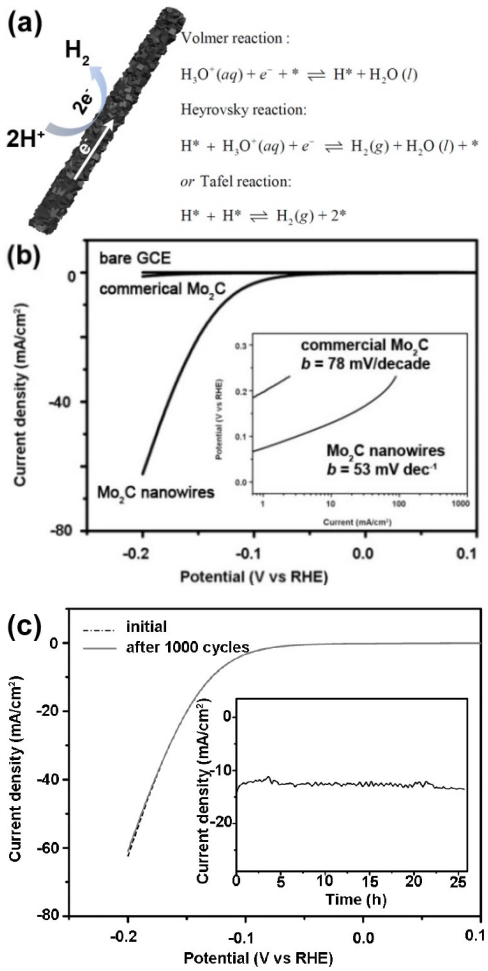

Fig. 2 (a) Schematic illustration for HER over Mo_2C nanowires. (b) Polarization curves obtained from glassy carbon electrodes modified with different Mo_2C catalysts (mass loading 0.21 mg cm^{-2}), and (inset of a) the corresponding Tafel plots recorded with the catalysts loading of 0.21 mg cm^{-2}; scan rate is 2 mV s^{-1}. (c) Stability for the Mo_2C nanowires modified electrode with initial LSV polarization curve and after 1000 cycles in 0.5 M H_2SO_4 at a scan rate of 10 mV s^{-1}. Inset is the time dependence of catalytic currents during electrolysis for Mo_2C nanowires in 0.5 M H_2SO_4 at η= 130 mV. Panels are reproduced with permission.[31] Copyright RSC (2014).

Advanced catalysts with element-abundance, economic-cost and stability are desired for electrochemical hydrogen evolution reaction (HER) to scale-up the promising clean energy of hydrogen.[32,33] We have recently explored the superior electrocatalytic properties of Mo_2C nanowires for HER from H_2O (Fig. 2a),[31] ensuring the good prospect to replace precious-metal catalysts inhibited by the scarcity and high cost.[34] The catalytic current ascribed to HER was observed at a low onset overpotential of ~70 mV (*vs.* RHE), and it rose rapidly at more negative potentials with current densities of ca. 60 mA cm^{-2} at η = 200 mV, about 50 times of that delivered by commercial Mo_2C (Fig. 2b). Meanwhile, a Tafel slope of ~53 mV dec^{-1} (Inset of Fig. 2b) indicated the obviously promoted Volmer step over Mo_2C. Additionally, the stability of catalytic response was satisfied. The catalyst afforded similar *i-V* curves to the initial cycle with negligible loss of activity even after 1000 cycles, and the current density around 12 mA cm^{-2} at a fixed overpotential of 130 mV was remained over 25 hours in time-dependence electrolysis (Fig. 2c).

Noticeably, the precursors of MoO_x/amine nanohybrids, e.g., $Mo_3O_{10}(C_6H_5NH_3)_2{\cdot}2H_2O$, possess tunable crystallographic structure, composition and morphology relying on the pH condition, molybdate concentration and amine species during solution-based synthesis,[35] indicating opened opportunities to further tailor the catalytic behaviors of Mo_2C. Various 1D and two-dimensional (2D) nanocatalysts of Mo_2C were derived from kinds of MoO_x/amine.[21] And their distinguishing performance associated with textural features, e.g., surface area, dispersibility, size and nanoporosity, were proved in the electrochemical HER from H_2O.[31]

The versatile design towards high efficient molybdenum-carbide electrocatalysts is well suggested by the above strategy. Wang *et al* have developed a series of nanoporous Mo_2C nanorods through the carburization of $Mo_3O_{10}(C_6H_5NH_3)_2{\cdot}2H_2O$ in H_2/Ar.[36] It was found that pure Mo_2C nanorods were obtained with 20 vol.% H_2/Ar at 700 °C, and metallic Mo phase emerged under 35 vol.% and 50 vol.% H_2/Ar flow because of the over-reduction of Mo_2C. Electrochemical test showed that Mo_2C contributed to the high catalytic activity, and Mo was inactive for HER due to its strong bond to atomic H. Decorated with Ni (30 wt.%), Mo_2C nanorods can be promoted comparable to Pt in alkaline condition. Leonard *et al* employed amine-metal oxide composites as the versatile precursors to fabricate various phases of molybdenum carbides (α-MoC_{1-x}, β-Mo_2C, η-MoC, and γ-MoC) towards HER.[37] Briefly, the hybrid obtained from an aqueous solution of ammonium molybdate and 4-Cl-o-phenylenediamine was heated under Ar flow at 750 °C for 12 h to form α-MoC_{1-x}, 850 °C for 12 h to form β-Mo_2C, and 850 °C for 24 h to form γ-MoC, respectively (Fig. 3a). And p-phenylenediamine was used to produce η-MoC at 1050 °C with zero dwell time. The electrocatalytic test showed that β-Mo_2C and γ-MoC possess the high HER activity with a much higher current density and lower overpotential than α-MoC_{1-x} and η-MoC (Fig. 3b). The satisfied activity of β-Mo_2C and γ-MoC should be ascribed to their valence band shape similar to that of Pt, as confirmed by XPS analysis. And the slightly lower density around Fermi level of γ-MoC than β-Mo_2C indicated the higher stability of γ-MoC in acidic solution.[38] Meanwhile, Mo_2C electrocatalysts have been also developed using biomass as precursors, e.g. common soybean proteins rich in carbon and nitrogen.[39] The derived catalysts containing 55% Mo_2C and 45% Mo_2N drove the HER at low overpotentials. The overpotential needed for driving a current density of 10 mA cm^{-2} (η_{10}) was ~177 mV, rivaling the performance of bulk Pt. And, thanks to the acid proof γ-Mo_2N phase, this catalyst was highly durable (> 500 hours) in a corrosive acidic solution.

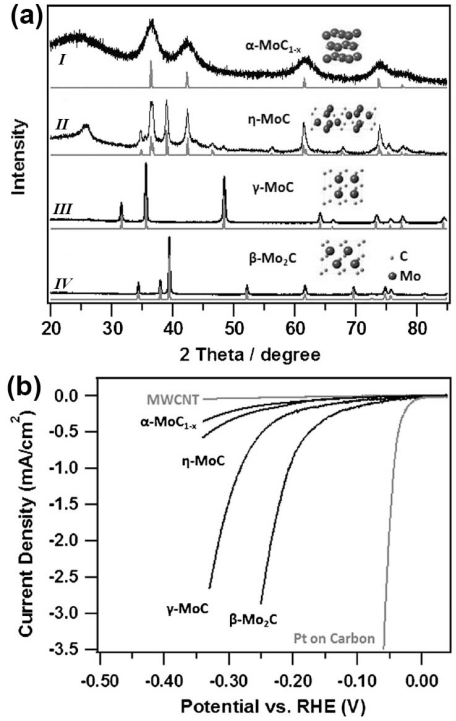

Fig. 3 (a) XRD patterns of I) α-MoC_{1-x} (JCPDS 01-089-2868), II) η-MoC (JCPDS 01-089-4305), III) γ-MoC (JCPDS 00-045-1015), and IV) β-Mo_2C (JCPDS 00-011-0608), and (b) the corresponding polarization curves in 0.1 M $HClO_4$ (mass loading 0.28 mg cm^{-2}). Panels are reproduced with permission.[37] Copyright Wiley (2014).

Other metal carbides highly active for HER have been also developed from organic-inorganic nanohybrids. Ham *et al* utilized the carburization of ammonium metatungstate and resorcinol-formaldehyde resin to yield W_2C microspheres with high surface area (176 m^2 g^{-1}), high chemisorption capacity and good activity for the HER.[40] In 1 M H_2SO_4 solution, the specific activity value reached 1.6 mA cm^{-2} at η = 100 mV, higher than that of commercial WC (0.09 mA cm^{-2} at η = 100 mV). Takanabe *et al* used mesoporous polymeric carbon-nitrides (C_3N_4) as the carbon source and template to synthesize nanocrystals of tungsten carbides.[41] Through the solid-state reaction of tungsten precursors embedded in reactive C_3N_4 matrix under inert flow, WC and W_2C nanoparticles with the size of ~ 5 nm were harvested at different temperature (Fig. 4a), which were examined in 0.5 M H_2SO_4 solution (Fig. 4b). Cathodic currents attributed to HER were observed for all carbides with an onset overpotential of approximately 100 mV. The sample WC-1223 (synthesized at 1223 K) exhibited the highest HER current among all of the samples with an onset overpotential of ~75 mV. The η_{10} on WC-1223 was found at 125 mV, comparable to Pt bulky catalysts. This synthetic strategy was further extended to tantalum carbide nanoparticles utilizing C_3N_4/Ta precursor under N_2 flow.[42] By altering the weight ratio of C_3N_4 template relative to Ta precursor at 1573 K, the formation of TaC, Ta_2CN, and TaN can be controlled. Electrochemical test revealed that the nanocatalysts were consistently able to produce hydrogen under acidic conditions (pH ~1), however carbides presented the lower activity than nitrides.

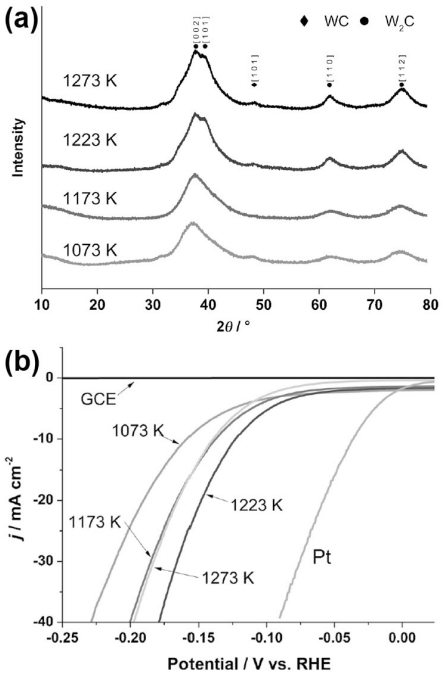

Fig. 4 (a) XRD patterns and (b) HER voltammograms of tungsten carbide product obtained at different temperature (mass loading 1 mg cm^{-2}). Panels are reproduced with permission.[41] Copyright Wiley (2013).

As for other catalytic reactions, various metal carbides have been fabricated from different organic-inorganic nanohybrids. For example, unsupported Mo_2C can be fabricated from Mo(VI)-hexamethylenetetramine (HMT),[20] $Mo(CO)_6$,[43] Mo(VI)-Melamine[44] etc., which were active for hydrodesulfurization (HDS) of dibenzothiophene,[20] and hydrogenation of naphthalene.[44]

The new system of "urea-glass route" established by Antonietti and Giordano *et al* is significant to prepare a wide variety of mono-dispersed metal-carbide nanoparticles based on amorphous hybrid precursors of metal-urea gels.[7,30,45] Starting from non-aqueous processes, homogenous gels composed of enriched M-O-C bonds reactive for carbide formation are generated via metal-chlorides reacting with urea in ethanol or methanol, and then, the nanosized carbides are finally obtained after calcination under inert flow.[7] Simply by adjusting the reaction conditions, the composition and structure of the products can be varied. It is needed to point out that the "urea-glass route" is also available for the preparation of metal-nitrides, especially in the low range of urea/metal ratio, which benefits the versatile design of metal carbides/nitrides heterostructures.[7] Another advantage is that the viscous gels are processable and can be operated into glassy film or porous matrix, thus enabling processes like spray coating, spinning, printing, or templating.[46,47]

Various nanosized carbides of Mo, W, Ti, Nb, V, Fe etc. have been achieved via this route,[7] which were used as efficient catalysts for oxidation, alkylation, and ammonia decomposition.[47-49] For example, Mo_2C and WC obtained via typical urea-glass route are active for benzyl alcohol oxidation.[48] Such catalysts exhibited the bifunctional nature to catalyze dehydrogenation and dehydration reactions, in which the relative ratio of reacting pathways can be tuned by a careful choice of the reaction conditions, such as the polarity of solvents. Mesoporous Fe_3C was fabricated through a modified

urea-glass route using silica nanoparticles as a hard template, which presented the high activity towards hydrogen production from ammonia decomposition.[47] The conversion of ammonia above 95% was found at 700 ◦C over mesoporous Fe_3C with the specific surface area of 415 m^2/g, while only ~ 50% conversion was observed on Fe_3C nanoparticles with the surface area of ~70 m^2/g. Meanwhile, the possibility to synthesize metal-carbide based materials with non-spherical morphologies and anisotropic shapes such as nanofibres can bring additional features to the final system. A simple two-step approach was established for the synthesis of chromium carbide nanofibers by means of an electrospinning technique.[46] In this procedure, urea/metal gels were shaped to fiber precursors and then thermally treated, resulting in two different types of fiber structures depending on the calcination temperature, which were active for the oxygen reduction reaction.

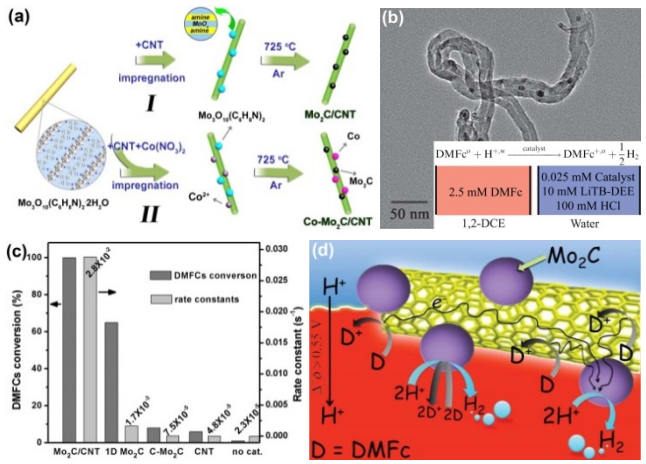

Fig. 5 (a) Schematic illustration for the fabrication of CNT-supported Mo_2C catalysts, and (b) TEM image of Mo_2C/CNT. Inset of (b) is the schematic representation of the initial compositions of the aqueous and organic phases, with the catalyst suspended at the interface, used to perform the biphasic H_2 evolution reaction. (c) Conversion rate of $[DMFc]^0$ to $[DMFc^+]$ after 600 s and the calculated apparent rate constants for the biphasic HER in the presence and absence of each catalyst. (f) Schematic of the biphasic H_2 evolution reaction in the presence of the conductive catalytic Mo_2C/CNT floating at a polarised interface. Panels are reproduced with permission.[50] Copyright RSC (2013).

Uploading nanosized metal carbides on supports with large surface will promote the highly-dispersed active sites and catalytic performance.[51] As for supported Mo_2C catalysts, several strategies have been introduced, including TPRe,[52] carbothermal hydrogen reduction,[53] and annealing mechanochemical,[54] which are, however, limited by the danger associated with using H_2, carbon deposition on carbide surface or difficulty in dispersion. Our synthetic strategy based on MoO_x/amine can be extended to supported Mo_2C catalysts.[29] Thermally stable carbon nanotubes (CNT) were used as the support, and $Mo_3O_{10}(C_6H_5NH_3)_2{\cdot}2H_2O$ precursor was loaded via a typical impregnation process (route I in Fig. 5a). After the following calcination, Mo_2C nanoparticles with the size of ~ 10 nm were uniformly loaded on CNT (Fig. 5b). Such a process was safer and more easily controlled than traditional TPRe and carbothermal hydrogen reduction methods due to the absence of H_2. The nanocomposites served as advanced catalysts for hydrogen evolution at a polarized water-1,2-dichloroethane interface, in which protons were pumped from the aqueous to the oil phase by the interfacial Galvani potential difference, and subsequently reduced to H_2 over Mo_2C/CNT by decamethylferrocene (Inset of Fig. 5b).[50] As shown in Fig. 5c, the superior activity of Mo_2C/CNT was demonstrated by the reaction rate constant of 2.88×10^{-2} s^{-1}, higher than that of Mo_2C nanowires (1.65×10^{-3} s^{-1}), commercial Mo_2C (7.5×10^{-5} s^{-1}) and CNT (4.8×10^{-5} s^{-1}). The highly-dispersed catalytic sites on Mo_2C/CNT were well indicated, and the support of CNT particularly acted as highly efficient conduits or "transport superhighways" for injected electrons to reach active Mo_2C (Fig. 5d).

This method was opened to load additive components to promote Mo_2C. If $Co(NO_3)_2$ was co-impregnated to CNT accompanying the hybrid precursor, the Co-modified Mo_2C/CNT (Co-Mo_2C/CNT) can be obtained (route II in Fig. 5a), in which the individual nanoparticles of Mo_2C and Co were well-dispersed on CNT (Fig. 6a).[29] In the catalytic methanol decomposition for H_2 production, Co was the key additive for stabilizing activity. As the liquid hourly space velocity (LHSV) of methanol was 1.5 h^{-1}, complete methanol conversion over Co-Mo_2C/CNT ($n_{Mo/Co}$ = 1.0) at 450 °C was noticeably maintained for 76 h with a H_2 selectivity above 90%, i.e., H_2 production rate of 2844 μmol min^{-1} g_{cat}^{-1} (Fig. 6b). Under LHSV of 1.0 h^{-1}, the high performance can be kept to 200 h with H_2 production rate of 1896 μmol min^{-1} g_{cat}^{-1}. In comparison, Mo_2C/CNT suffered an obvious deactivation after 10 h of reaction, and Co/CNT displayed the low H_2 selectivity of 40%. The effect of Co was ascribed to its ability to turn carbon-deposition on Mo_2C to CNT, maintaining the high activity towards H_2 production,[55] which were well confirmed by the TEM investigation carried out after a methanol stream at 450 °C (Fig. 6c-6e).

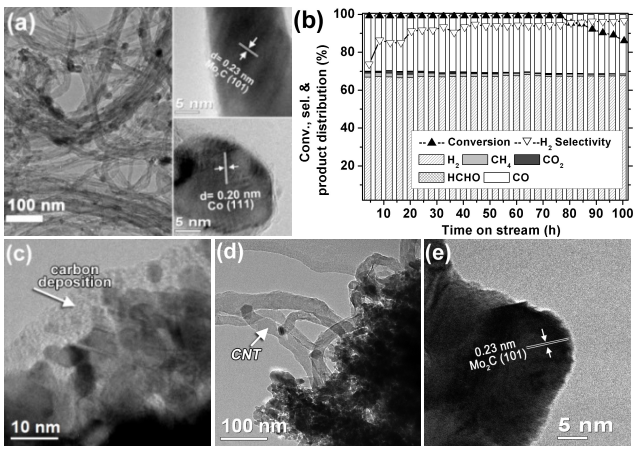

Fig. 6 (a) TEM images of Co-Mo_2C/CNT. Insets of a are the TEM images of Mo_2C and Co nanoparticles. (b) Performance of producing H_2 from methanol decomposition over Co-Mo_2C/CNT (6.0%, Mo/Co = 1.0) at 450 °C with time on steam (LHSV =1.5 h^{-1}, m_{cat} = 1.0 g). TEM images of the carbon deposition on (c) Mo_2C and (d) Co-Mo_2C catalysts after treatment under CH_3OH/Ar at 450 °C in a tubular reactor for 8 h; and (e) is the HRTEM image of Mo_2C surface in Co-Mo_2C after methanol treatment. Obviously, a layer of deposited carbon was easily observed in Mo_2C, while, only CNT, but not heavy coke, was formed on the surface of Mo_2C with Co-modification. Panels are reproduced with permission.[29] Copyrights RSC (2010).

As for supported tungsten carbide, similar strategy has been developed by Nakanishi *et al* utilizing a tungsten acid/polymer hybrid as precursors (Fig. 7a).[56] The polymerization of polydiaminopyridine (PDAP) released protons to react with Na_2WO_4, resulting in nanohybrids composed of PDAP and insoluble H_2WO_4 nanoparticles. The hybrids were pyrolyzed in

the presence of iron to form N-rich tungsten carbonitrides (Fe-WCN). As indicated by TEM investigation (Fig. 7b and 7c), numerous nanoparticles of ca. 10–20 nm in diameter were uniformly loaded on carbon nitride nanospheres (~500 nm). As compared with the reference catalysts of CN, FeCN and WCN, Fe-WCN displayed the remarkably increased HER activity (Fig. 7d), which was ascribed to the low resistance (0.5 Ω cm) and large surface area (127.2 m^2 g^{-1}). An onset overpotential of about 100 mV, a current density of 10 mA cm^{-2} at η = 220 mV and a Tafel slope of 47 mV dec^{-1} were observed on Fe-WCN in acidic medium, comparable to the most cost-effective electrocatalysts. XPS analysis (Fig. 7e) confirmed the lower-energy shift with increasing pyrolysis temperature due to the loss of N content in Fe-WCN, which suggests the W-bound N species substantially decreased the electron density of W atoms, and thus downshift the d band of W active sites to promote the combination of H_{ad} to H_2.

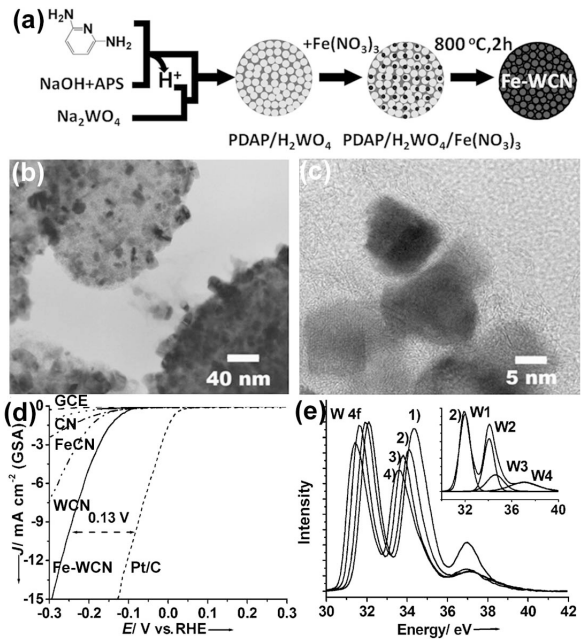

Fig. 7 (a) Synthesis of Fe-WCN nanocatalysts from H_2WO_4/PDAP nanohybrids. (b, c) TEM images of Fe-WCN synthesized at 800 °C. (d) HER polarization curves of glassy carbon, CN-800, FeCN, WCN-800, Fe-WCN-800, and commercial Pt/C catalyst in a pH 1 medium (mass loading 0.4 mg cm^{-2}). (e) W 4f spectra of Fe-WCN catalysts prepared at various temperatures. (1) Fe-WCN-700, (2) Fe-WCN-800, (3) Fe-WCN-900, and (4) Fe-WCN-1000. The inset shows the deconvoluted XPS W 4f spectra of (2) Fe-WCN-800. W1 and W2 are N-bound Watoms, W3 and W4 are O-bound W atoms. Panels are reproduced with permission.[56] Copyright Wiley (2013).

The strategy towards metal-carbides loaded on supports with large surface has been proved effective based on the controlled evolution from organic-inorganic nanohybrids. Various highly active catalysts of mesoporous MoOC/C,[57] $W_{1+x}C$/C nanospheres,[58] WC/graphitic-carbon,[59] and mesoporous WC/C,[60] have been developed for the applications in electrocatalysis, ammonia decomposition and hydrogenation treatment of petroleum chemicals, in which the enriched interaction between well-dispersed active sites and supports advanced the efficient catalytic conversion. The tunable synthesis based on well-defined organic-inorganic nanohybrids presented the convenience to achieve the high-performed carbide catalysts.

III. Metal nitrides

As another class of noble-metal-like catalysts, metal nitrides have also attracted much attention. For example, Mo_2N, W_2N, Ni_3N and Fe_3N are promising for hydrogen-involving catalytic reactions, e.g., HDS and hydrodenitrogenization (HDN).[61] In order to avoid the using of corrosive NH_3 or flammable H_2 at high temperature for nitridation,[18,62] easy strategies have been developed from organic-inorganic hybrids containing N-rich organic components. Well-dispersed Mo_2N with lamellar morphology and large surface has been prepared from the direct decomposition of $(HMT)_2(NH_4)_4$-Mo_7O_{24} (HMT = hexamethylenetetramine) at 550-800 °C.[63] During decomposition, the reduction of Mo species by HMT ligand occurred, with the release of CO gas. Moreover, bimetallic nitrides highly active in HDN reaction, such as Co_3Mo_3N and Ni_2Mo_3N, were further developed from Co- and Ni-salt modified $(HMT)_2(NH_4)_4$-Mo_7O_{24}, respectively.[64,65] Such bimetallic nitrides showed substantial synergic effect between Ni or Co and Mo.

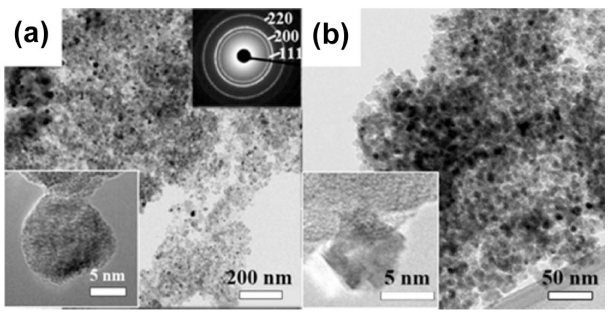

Fig. 8 TEM pictures of (A) TiN and (B) TiN-Ni. Panels are reproduced with permission.[66] Copyright ACS (2014).

The "urea-glass route" is significant for the design of metal nitride nanostructures due to the convenient modulation on the structures and properties of products employing a wide variety of N-rich organic molecules, e.g., urea, dicyandiamine, cyanamide, polypeptide, hydrazine etc.[7] Giordano *et al* reported the successful synthesis of a series of metal nitrides, including W_2N, Mo_2N, NbN, CrN, TiN, GaN, VN and ZrN.[7,30,45] The catalytic properties and application have been highlighted associated with their structural features. Sponge-like Ni_3N nanostructures were fabricated via ionothermal process using Ni/dicyandiamine as the precursor, which showed the good activity for hydrogenation of nitrobenzene to aniline.[67] Similarly, the pyrolysis of a Fe-polypeptide under a N_2 atmosphere, typically at 700 ^oC, has been utilized to prepare sponge-like Fe_3N with enriched porosity, which were active for ammonia decomposition.[68] Furthermore, as supports in heterogeneous catalysts, semiconducting nitrides would modify the electron density and thus activity of the supported metal (Mott−Schottky effect).[69] The TiN nanoparticles obtained via urea-glass route were introduced as support to enhance the catalytic activity of Ni for the hydrogenolysis of lignin-derived aryl ethers.[66] The well-defined nanostructures with large surface area (> 200 $m^2\ g^{-1}$) enhanced the activity of Ni via their enriched interaction. TEM investigation showed small and monodisperse primary TiN nanoparticles and TiN-Ni composites obtained after Ni addition (Fig. 8). A comparison of TiN-Ni with pure TiN or Ni particles during hydrogenolysis was performed to elucidate the synergic effect between the two components in the nanocomposites, as shown in Table 1. The hydrolysis of benzyl-phenyl ether 1 was studied as a model for the α-O-4 linkage in lignin. TiN did not show detectable conversion (entry 1). Ni nanoparticles were effective in promoting this hydrogenolysis, and despite the low activity up to 125 °C, 90% conversion could be obtained at 150 °C (entries 3 and 4). Nevertheless, TiN-Ni composite showed a superior activity affording full conversion already at 125 °C (entry 6), with phenol and toluene as the sole products. Meanwhile, the cleavage of the alkyl aryl ether bond in phenylethyl-phenyl ether 2, as a model for β-O-4 linkages in lignin, occurred under more severe conditions, in line with its higher dissociation energy compared to 1. TiN and Ni particles showed no activity even up to 150 °C. However, TiN-Ni catalyst presented a conversion of 65% at 150 °C with a flow rate of 0.5 mL min^{-1}, while full conversion could be achieved using a lower volumetric flow (0.3 mL min^{-1}, entries 9 and 10). Accordingly, the better activity and selectivity of TiN-Ni has been confirmed in the hydrogenolysis of diphenyl ether, which is one of the strongest ether bonds in lignin. This well-indicated synergic catalysis between TiN and Ni would pave the way to new competitive lignin refining strategies based on relatively cheap and abundant materials.

On the other hand, it is significant that the bulk (e.g., electronic and optic) and surface (e.g., acid and base) properties of metal nitrides are associated with nitridation levels.[61,70] As been commonly accepted, the introduction of N into metal oxides can increase valance-band energy and narrow band gap to thus enhance catalytic activity.[5,6] In the case of tantalum, a series of TaO_xN_y and Ta_3N_5 with smaller band-gap energy (*vs.* Ta_2O_5), enriched defective nitrogen species, and abundant oxygen vacancies, are highly active in the catalytic processes of hydrogenation and visible-light-driven water splitting.[71,72] Such tunable electronic properties highlights the importance of a method to synthesize (oxy)nitrides with tailored composition. Unfortunately, the controlled nitridation is difficult via current strategies due to the high rate of nitridation.[18,73] By-products of Ta_3N_5, Ta_4N_5, and even TaN are easily generated from uncontrollable nitridation of TaON. Although urea and cyanamide have been reported as safe nitrogen sources for

Table 1. Effect of Ni, TiN and TiN-Ni catalysts on hydrogenolysis of different lignin model molecules. Panels are reproduced with permission.[67] Copyright ACS (2014).

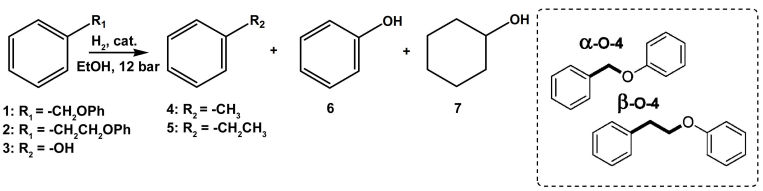

entry	cat.	sub.	T (^oC)	con. (%)	sel. (%)[c] 4	5	6	7	Productivity (mmol $h^{-1}\ g_{cat}^{-1}$)
1[a]	TiN	1	150	0	—	—	—	—	—
2[a]	Ni	1	100	0	—	—	—	—	—
3[a]	Ni	1	125	18	51	—	49	—	0.225
4[a]	Ni	1	150	90	57	—	43	—	1.282
5[a]	TiN-Ni	1	100	67	53	—	47	—	0.666
6[a]	TiN-Ni	1	125	>99	54	—	46	—	1.013
7[a]	TiN	2	150	0	—	—	—	—	—
8[b]	Ni	2	150	0	—	—	—	—	—
9[a]	TiN-Ni	2	150	65	—	57	—	43	0.695
10[b]	TiN-Ni	2	150	>99	—	54	—	46	0.608
11[b]	TiN-Ni	3	150	55	—	—	—	100	0.620

[a] Conditions: 0.05 M solution of starting material in EtOH, 12 bar, 0.5 mL min^{-1}. [b] 0.3 mL min^{-1}. [c] Determined by GC-MS analysis.

preparing tantalum nitrides, only impure and deeply reduced TaN could be obtained, as an effective control on reactions is absent.[74,75]

We discovered that the controlled release of active N-source from urea was important for nitridation in the typical "urea route". As a further controlled version of urea pyrolysis, a new Ca^{2+}-assisted urea route was proposed for the controllable synthesis of well-defined TaON and Ta_3N_5 nanoparticles, which were mono-dispersed, well-separated, mostly single crystalline, and free from organic stabilizers.[22] The controlled-nitridation mechanism associated with the chelation between Ca^{2+} and urea was further proved available for Zr-based (oxy)nitrides. It's interesting that the metastable phase of γ-TaON was even received at the low urea/Ta mole ratio of 2.0, which would easily convert to baddeleyite-type β-TaON.[76] Its synthesis usually requires the moderate conditions with precisely-controlled temperature and pressure. In the medium of molten $CaCl_2$, the formation and stabilization of γ-TaON can be easily achieved probably because of the rich chemical interactions between Ta with Ca^{2+}.

Owing to the difficulty to thoroughly remove Ca-species (e.g., $Ca_2Ta_2O_7$), SiO_2 nanoparticles were introduced as another efficient assistant agent, which can even be used as supports for active (oxy)nitride nanoparticles.[23] During heating, the pyrolysis of urea into carbon-nitride species (CN_x) was promoted by Si-OH group on SiO_2 surface at mild temperature, and the as-formed CN_x could further acted as a slowly-releasing N-source for controlled nitridation (Scheme 2). The assistant and hard-template, SiO_2 nanoparticles, can be removed by the treatment with NaOH solution. Following this mechanism, the production of TaON over Ta_3N_5 nanoparticles with well-defined composition and size was achieved through varying urea/Ta ratio in gel precursors (Fig. 9; TaON, $R_{urea/Ta}$ = 1.5; Ta_3N_5, $R_{urea/Ta}$ = 3.0). The electronic properties of Ta were tailored by the different nitridation levels in such nanoparticles, as confirmed by XPS, which significantly improved the activity for alkene epoxidation with H_2O_2, compared with Ta_2O_5. The activity of Ta_3N_5 nanoparticles was best; however, the selectivity was only 78% due to the following hydration of epoxides by strong basicity on Ta_3N_5. The basicity resulting from nitridation can be varied by acid treatment, after which the selectivity was obviously increased to 86%. This is the first time to discover that nitirdation can remarkably improve epoxidation activity because of the easier electron transfer from N (*vs.* O) to Ta, and also result in tunable basicity important for reaction pathway (Scheme 3). This opens up opportunities to develop superior nitride-based catalysts for selective oxidation, especially for reactions involving cheap O_2 as the oxidant. However, such (oxy)nitrides synthesized so far are inactive for O_2 activation.

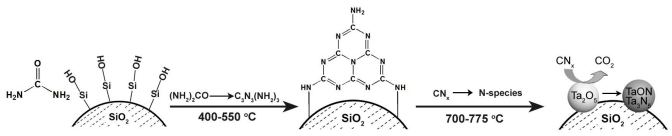

Scheme 2 Illustration of SiO_2-surface-assisted mechanism for controllable synthesis of TaON and Ta_3N_5 nanoparticles through CNx-intermediate process catalyzed by SiO_2.[23] Copyrights Wiley (2012).

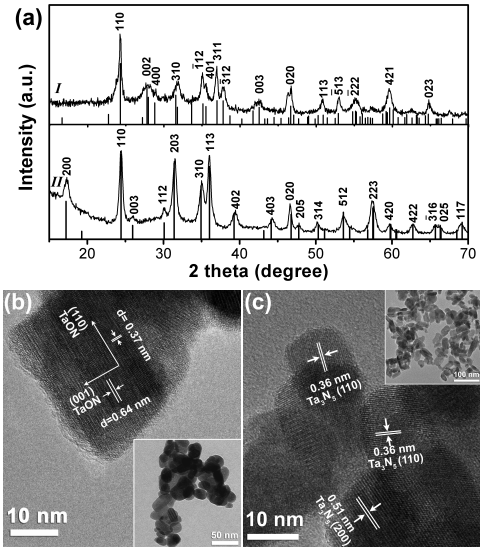

Fig. 9 (a) XRD patterns of (I) TaON and (II) Ta_3N_5 nanoparticles obtained by SiO_2-assisted urea method with $R_{U/Ta}$ of 1.5 and 3.0, and (b, c) their corresponding TEM images. Panels are reproduced with permission.[23] Copyrights Wiley (2012).

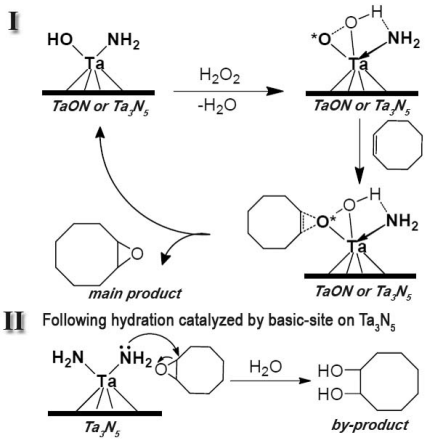

Scheme 3 Catalytic mechanism for (I) epoxidation of cyclooctene by TaON and Ta_3N_5 nanoparticles, and (II) overreaction of hydration to diol-products catalyzed by the basic site on Ta_3N_5. Panels are reproduced with permission.[23] Copyrights Wiley (2012).

A new MoS_2/Ta_3N_5 catalyst integrating Ta_3N_5 nanoparticles with ultrathin MoS_2 layers on nanoscale has been developed.[77] Employing MoS_2 nanolayers as a biomimetic O_2-activation agent, MoS_2/Ta_3N_5 showed high activity and selectivity in the aerobic oxidation of alcohols, as a result of the synergistic effect between MoS_2 and Ta_3N_5 (Scheme 4). The efficiency of the conversion of alcohols into aldehydes was well confirmed in a wide range from benzylic alcohols to aliphatic and alicyclic alcohols, delivering a high selectivity near 99% (Table 2). Such nanocatalysts were also active in the aerobic oxidation of alkenes, amines, and sulfides. More importantly, the different activities respecting various substrates implied the potential use of this catalyst for multifunctional substrates. For example, high selectivity for hydroxy-group (>90%) was observed in the oxidation of unsaturated alcohols. As a good example, this work of Ta-nitrides illustrates a broadly applicable protocol to tailor electronic and catalytic properties via controlled nitridation.

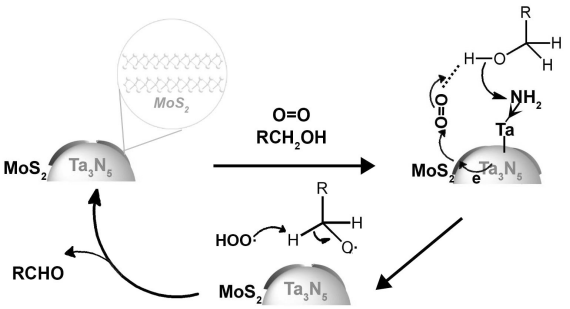

Scheme 4 Schematic illustration of alcohol aerobic oxidation over MoS_2/Ta_3N_5 nanocatalysts. Panels are reproduced with permission.[77] Copyrights Wiley (2012).

Table 2 Selective oxidation of alcohol.[a] Panels are reproduced with permission.[77] Copyrights Wiley (2012).

Entry	Substrates	Sel. (%)	Conv. (%)	t (h)
1	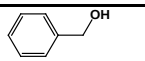	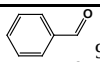 99	85	1.5
2	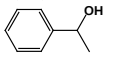	 99	88	1.5
3	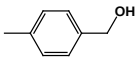	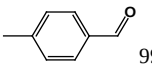 99	99	1.5
4	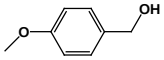	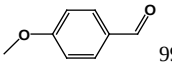 99	99	1.5
5	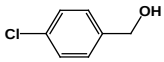	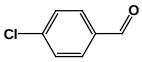 96	74	1.5
6	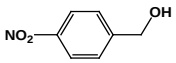	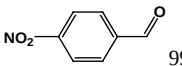 99	36	1.5
7	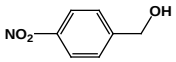	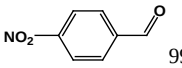 99	86	3.0
8	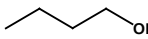	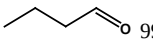 99	80	4.0
9	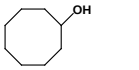	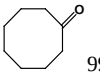 99	80	2.0

[a] Reaction condition: alcohol (1 mmol), MoS_2/Ta_3N_5-5.0 (40 mg), N, N-Dimethylacetamide (4 mL), O_2 balloon (1 atm.), 120 °C.

IV. Metal sulfides and selenides

Compared with carbides and nitrides, metal sulfides and selenides can be synthesized at lower temperature (< 350 °C). Solution-based routes have been introduced to their fabrication.[78] The organic-inorganic hybrids with tunable composition and specific structures not only facilitate the formation and growth of sulfides and selenides, but also promote the design of relevant hierarchical or anisotropic nanostructures via the controlled morphology-transformation of precursors.

The organic-inorganic hybrids containing desired metals and chalcogens in a single molecule have been utilized as the single-source precursors (SSP) for the synthesis of metal chalcogenides. The organic fragments in such coordination metal complexes are removed, and metal chalcogenides are reassembled under mild conditions.[79] This SSP strategy permits a reproducible production of single-crystalline, mono-dispersed and pure nanocrystals. O'Brien *et al.* have prepared iron sulfide nanoparticles via decomposing bis(tetra-*n*-butylammonium) tetrakis[benezenethiolato-μ_3-sulfidoiron] ($[N^nBu_4]_2[Fe_4S_4(SPh)_4]$) in different solvents.[80] And the phase change from pyrrhotite type Fe_7S_8 to greigite type Fe_3S_4 was found when temperature was varied from 180 °C to higher ones (e.g., 200, 215 and 230 °C). Other nanosized iron sulfides can be obtained from different precursors. For example, Fe_7S_8 nanosheets and FeS_x nanoribbons were received by pyrolyzing Fe(diethyldithio-carbamate)$_2$(1,10-phenanthroline) (Fe(Ddtc)$_2$(Phen)) in oleylamine and oleylamine/1-octadecane, respectively.[81] Their different growth was ascribed to the selective adsorption of capping ligands on specific crystal planes. Vittal *et al.* further developed the SSP to synthesize highly mono-dispersed nanoparticles of CdS, Ag_2Se, $CuInS_2$, etc.[82-84] Moreover, the controlled decomposition of SSP and the consequent anisotropic growth can be realized by solution-liquid-solid mechanism,[85] in which the commonly used Bi and In nanoparticles catalyze metallo-organic precursors decomposition, and lead to 1D growth on the basis of the binary-phase transfer involving objective metal-chalcogenides. A series of 1D sulfides and selenides, e.g., PbS, CdS, CdSe, PbSe, $PbSe_xS_{1-x}$, etc., have been achieved via such strategy.[86-88] It is significant that the textural features (e.g., diameter, length and composition) and consequent optic and electronic properties are tunable in a wide range by the control over catalytic nanoparticles and relevant phase behaviors, highlighting them as functional segments for solar cells, photocatalysis, sensor and photodetectors.[85]

More importantly, the organic-inorganic nanohybrids with well-defined morphology can be utilized to explore anisotropic or hierarchical nanostructures of metal sulfides and selenides via easily-controlled evolutions. For example, Rao *et al.* prepared $Fe_{1-x}S$(ethylenediamine)$_{0.5}$ nanowires by reacting $FeCl_2{\cdot}4H_2O$ with CH_3CSNH_2 at 180 °C.[89] And, after heating to 200-300 °C, $Fe_{1-x}S$ nanowires were easily received. Similarly, pure Fe_7S_8 nanowires were generated from $Fe_{18}S_{25}$(triethyleneteramine)$_{14}$ nanoribbons at 800 °C under Ar flow.[90]

Exploring anisotropic nanostructures of transition-metal chalcogenides from organic-inorganic nanohybrids are considered as new approaches towards promising oxygen-reduction-reaction (ORR) electrocatalysts with desirable morphology, size, composition and surface-decoration. Yu *et al.* carried out a series of study on the structural design of $CoSe_2$-based electrocatalysts.[91-93] With amine molecules as structure-directing agents, hybrid nanobelts of $CoSe_2$-amine (amine = diethylenetriamine (DETA), triethyleneteramine (TETA) and tetraethylenepentamine (TEPA)) were successfully obtained in a binary solution.[94] Used as the electrocatalyst for cathodic OOR, the $CoSe_2$-DETA bore the onset potential of ca. 0.71 V in 0.5 M H_2SO_4 electrolyte.[92] To further improve the activity and stability, research has focused on the combination with other functional nanoparticles utilizing the synergetic effects in catalyst/support. In a polyol reduction in acid solution, the copious surface amino groups on $CoSe_2$-DETA allowed the loading of highly dispersed Fe_3O_4, and the amine molecules were removed by H^+, resulting in $Fe_3O_4/CoSe_2$ nanobelts. They showed better catalytic activity than the original $CoSe_2$-DETA, in which the onset potential and current density were increased by 0.05 V and 1.01 mA cm^{-2} (at 0.3 V, 1600 rpm), respectively. The number of electrons transferred also increased from 2.1 to 3.6. XPS spectra confirmed the shift of Co $2p_{3/2}$ binding-energy from 778.5 to 777.8 eV after decoration, possibly due to the electron transfer from Fe_3O_4 to $CoSe_2$. This would lead to oxygen vacancies on the interfacial oxides, the new active sites for O_2 absorption and activation. Such mechanism was further applied to constructing $Mn_3O_4/CoSe_2$ nanocatalysts displaying good stability and excellent activity for oxygen-evolution-reaction from water.[93] Moreover, the $CoSe_2$-DETA also served as the precursors for Pt/$CoSe_2$ nanobelts (Fig. 10a) used in ORR.[91] Beyond the greatly improved activity in comparison with

original $CoSe_2$-DETA (Fig. 10b), they displayed prominent methanol-tolerance for ORR, which successfully overcame the easy decrease of cathode potential and fuel efficiency in many cases of Pt-based catalysts as methanol molecules crossed over from the anode to the cathode side through polymer membranes.[95] Over commercial Pt/C catalyst, the ORR activity was obviously reduced in the presence of methanol even at a low concentration of 0.05 M (Fig. 10c). However, the ORR onset potential and current density for $Pt/CoSe_2$ remained almost unchanged with different concentrations of methanol. Even at a high concentration of 5 M, the reduction in ORR activity was still negligible (Fig. 10d). Such excellent stability of $Pt/CoSe_2$ at high methanol concentrations was attributed to the use of $CoSe_2$ supports and their synergy with Pt nanoparticles.

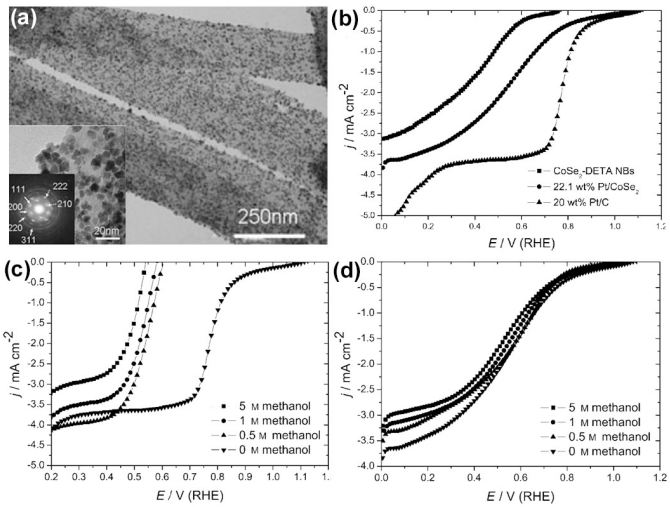

Fig. 10. (a) TEM images of $Pt/CoSe_2$ nanobelts. (b) Polarization curves for ORR on pristine $CoSe_2$-DETA, 22.1 wt% $Pt/CoSe_2$, and 20 wt% Pt/C catalyst in O_2-saturated 0.5 M H_2SO_4 solutions. Polarization curves for ORR on (c) 20 wt% Pt/C catalyst and (d) 22.1 wt% $Pt/CoSe_2$ in O_2-saturated 0.5 M H_2SO_4 electrolyte containing 0, 0.5, 1, and 5 M methanol. Panels are reproduced with permission.[91] Copyrights Wiley (2011)

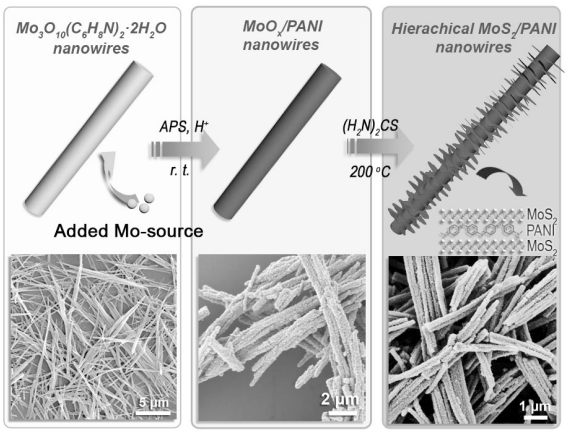

Scheme 5. Scheme for the fabrication of hierarchical MoS_2/PANI nanowires through facile polymerization and hydrothermal-treatment of $Mo_3O_{10}(C_6H_8N)_2 \cdot H_2O$ precursor. Panels are reproduced with permission.[25] Copyrights Wiley (2013).

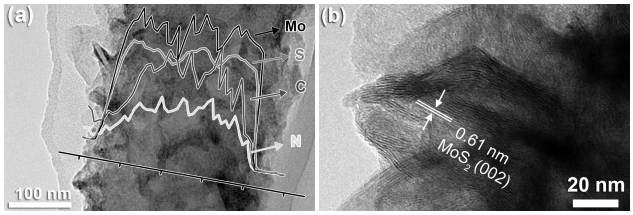

Fig. 11. (a) TEM image with elemental (Mo, S, C, and N) distribution and (b) HR-TEM image of a MoS_2/PANII nanowire. Panels are reproduced with permission.[25] Copyrights Wiley (2013).

The organic-inorganic hybrid precursors further suggest the rational design of hierarchical metal sulfides and selenides nanostructures via tailoring the relationship between the morphology evolution of original precursor and the formation of the target sulfides or selenides. A series of lead chalcogenide nanotubes have been fabricated via the controlled evolution of Pb-cysteine nanowires.[96] Pb-cysteine plays crucial roles as both the lead source and the template, in which the equilibrium between nanowire dissolution and chalcogenide nanoparticle formation should be controlled to achieve the hollow architecture. Meanwhile, MoO_x/amine with tunable composition and structure would benefit the fabrication of MoS_2-based hierarchical nanostructures.[35] The evolution from $Mo_3O_{10}(C_6H_5NH_3)_2 \cdot 2H_2O$ nanowires composed of aniline monomer to a series of MoO_x/PANI (PANI = polyaniline), e.g., nanotubes, nanowires, and rambutan-like nanoparticles, have been achieved by simply modulating pH condition during polymerization,[97] which can further evolve to hierarchical MoS_2. After an easy hydrothermal treatment of MoO_x/PANI nanowires with thiourea at 180 °C, the MoO_x was successfully converted to MoS_2 nanosheets, while the PANI matrix and 1D morphology were maintained, resulting in the hierarchical MoS_2/PANI nanowires composed of 2D MoS_2 (Scheme 5).[25] Such formation was associated with the growth habit of MoS_2 and the hybrid features of 1D precursor, in which the anisotropic growth of 2D MoS_2 was owing to its layered structure held by van der Waals interactions, and the soft and flexible chains of PANI can buffer the volume expansion and thus preserve the wire-like morphology during sulfidation. Furthermore, hierarchical MoS_2-C nanowires and nanotubes have also been fabricated by the sulfidation of MoO_x/PANI nanowires by H_2S at 400 °C.[98] Such hierarchical compsoites with ultrathin MoS_2 evenly integrated by conducting PANI (Fig. 11) or C matrix has showed the superior performance as electrode for Li ion batteries.[25,98] It is also expected that the surface activity and related catalytic behavior would be enhanced due to the hierarchically assembling active MoS_2.

Zhang *et al* proposed the synthesis of hierarchical nanosheet-based MoS_2 nanotubes (HNN-MoS_2) from MoO_3-ethylenediamine nanowires ($Mo_3O_{10}(C_2H_{10}N_2)$, ethylenediamine trimolybdate), as shown in Fig. 12a.[24] The UV/Vis diffuse reflectance spectra of HNN-MoS_2 showed a stronger and wider adsorption from 420 to 800 nm than commercial MoS_2 (Fig. 12b). The improved photocurrent-density responses were well detected on HNN-MoS_2, which delivered the short-circuit photocurrent density of 0.09 mA cm^{-2}, nearly 9 times higher than that of commercial MoS_2 (Fig. 12c). The significantly improved activity and stability of such hierarchical MoS_2 were well confirmed in the application of photoelectrocatalytic water splitting and electrocatalytic HER. In the very recent work, we conducted the facile synthesis of hierarchical MoS_2/C nanospheres in the hydrothermal system of ammonium heptamolybdate tetrahydrate, thiourea and glucose.

The *in-situ* generated polysaccharides act as an effect template to confine the growth of MoS_2, resulting in the rim-site enriched ultrathin nanosheets embedded in conducting carbon after carbonization. Because of the abundant active sites on MoS_2 nanosheets and the improved conductivity by conducting carbon, the as-synthesized MoS_2/C nanospheres exhibit remarkably enhanced performance for electrochemical HER. The above work, as good examples, would open up new opportunities for developing efficient, economic and stable photocatalysts and electrocatalysts of chalcogenides based on organic-inorganic nanohybrids.

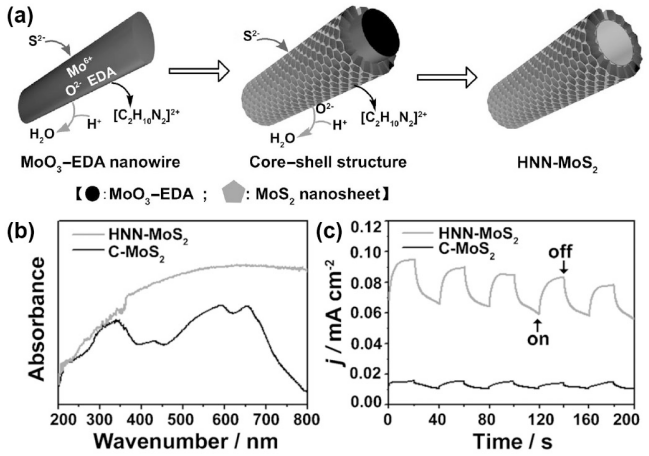

Fig. 12 (a) Schematic representation of the synthesis of hierarchical nanosheet-based MoS_2 nanotubes (HNN-MoS_2; cross-section view) through the anion-exchange reaction of the inorganic–organic MoO_3–EDA hybrid nanowires with S^{2-} at elevated temperature. (b) UV/Vis diffuse reflectance spectra and (c) photocurrentdensity response at an applied bias of 0.6 V versus SCE under visible light illumination (λ > 420 nm) of the as-prepared hierarchical MoS_2 nanotubes (HNN-MoS_2) and commercial MoS_2 samples (C-MoS_2). Panels are reproduced with permission.[24] Copyrights Wiley (2013).

V. Conclusion and Outlook

This contribution highlights the recent advances on the fabrication of metal non-oxide nanocatalysts (e.g., carbides, nitrides, sulfides and selenides) from organic-inorganic nanohybrids and their catalytic applications in hydrocarbon conversion, hydrogen production, and electrocatalytic HER and ORR, as summarized in Scheme 6. As for metal carbides and nitrides requiring high-temperature (> 700 ^{o}C) for synthesis, the organic-inorganic nanohybrids provide the quasi-homogeneous reactions between organic and inorganic molecules on nanoscale, significantly avoiding the disadvantage of gas-solid interface processes in traditional TPRe methods. With easy control over hybrid precursors and their evolution during calcination, the morphology, composition and crystalline structure of carbides and nitrides can be tailored to achieve the highly-improved catalytic performance. Moreover, the organic-inorganic nanohybrids were not only used as the source for fabricating nanosized metal sulfides and selenides, but also utilized as the key precursors towards the anisotropic or hierarchical nanostructures with enhanced functionalities. A wide range of metal sulfide and selenide nanostructures have been explored, and they exhibited obviously improved electrocatalytic activity due to the synergistic enhancement. Remarkably, the merits of design strategies in this feature article are highlighted as the resultant nanomaterials with hierarchical structures, precise-controlled properties and superior catalytic performance, as well as the easy preparing processes.

It was noticed that the controlled evolution of organic-inorganic nanohybrids to functional metal non-oxides is the key for achieving high-performed nanocatalysts, in which there are still two challenges. Firstly, during the conversion of organic-inorganic nanohybrids to metal non-oxides, the rate equation between competitive reactions, including formation of metal non-oxides, conversion of organic molecules, deformation of precursor, and crystal growth of products, should be taken in account for the design of metal non-oxide catalysts. Thus, the clear mechanism underlying evolutions is greatly demanded in further investigation based on *in-situ* methods. Secondly, a new system for versatile organic-inorganic nanohybrids is desirable to provide more suitable precursors for non-oxide design, which demands the synthetic strategies focusing on their interface interaction and consecutive crystal growth.[99-101] More importantly, such achievement would pave the way for robust metal phosphides, other kind of important non-oxide catalysts towards HDS and HER.[102-105] With rational design and delicate control in synthesis process, this unique class of strategies may overcome some bottlenecks in the development of efficient catalysts towards efficient energy conversion and storage.

Acknowledgements

We are grateful for the financial support from the 973 Program (2013CB934101), NSFC (21203075, 21373102 and 21433002), STCSM (11JC1400400) and Guangdong Higher Education Institute (YQ2013022 and KLB11003).

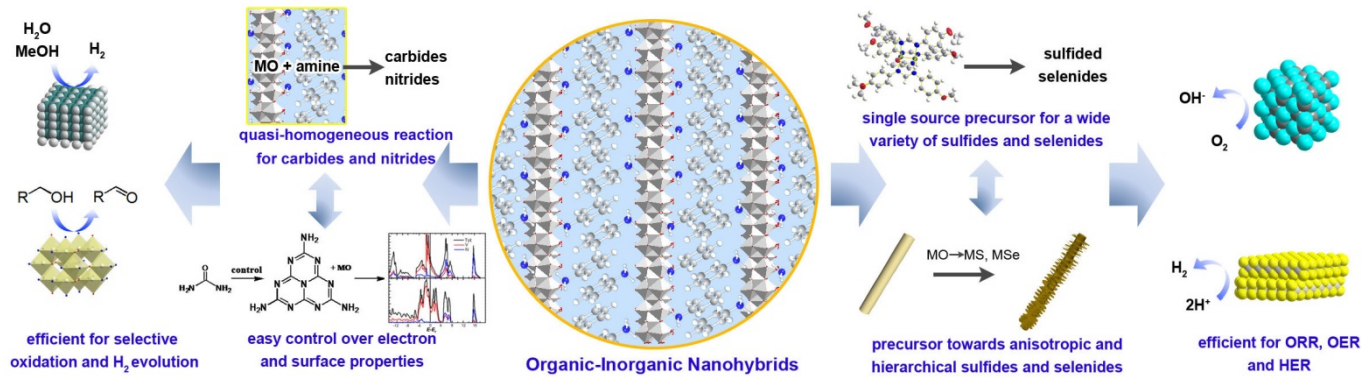

Scheme 6. Summarized illustration for the synthesis of metal carbides, nitrides, sulfides and selenides from organic-inorganic nanohybrids.

Notes and references

[a] Department of Chemistry, Jinan University, 510632 Guangzhou (China)
E-mail: tqsgao@jnu.edu.cn
[b] Department of Chemistry and Shanghai Key Laboratory of Molecular Catalysis and Innovative Materials, Fudan University, 200433 Shanghai (China)
E-mail: yitang@fudan.edu.cn

1 H. H. Hwu, J. G. Chen, *Chem. Rev.*, 2005, **105**, 185.
2 A. M. Alexander, J. S. Hargreaves, *Chem. Soc. Rev.*, 2010, **39**, 4388.
3 M. Chhowalla, H. S. Shin, G. Eda, L. J. Li, K. P. Loh, H. Zhang, *Nat. Chem.*, 2013, **5**, 263-275.
4 A. Costales, M. A. Blanco, A. M. Pendas, A. K. Kandalam, R. Pandey, *J. Am. Chem. Soc.*, 2002, **124**, 4116-4123.
5 R. Asahi, T. Morikawa, T. Ohwaki, K. Aoki, Y. Taga, *Science*, 2001, **293**, 269-271.
6 K. Maeda, K. Domen, *J. Phys. Chem. C*, 2007, **111**, 7851-7861.
7 C. Giordano, M. Antonietti, *Nano Today*, 2011, **6**, 366-380.
8 N. Ji, T. Zhang, M. Y. Zheng, A. Q. Wang, H. Wang, X. D. Wang, J. G. G. Chen, *Angew. Chem. Int. Ed.*, 2008, **47**, 8510-8513.
9 V. Heine, *Phys. Rev. A*, 1967, **153**, 673.
10 E. Furimsky, *Appl. Catal. A*, 2003, **240**, 1-28.
11 C. Yang, H. B. Zhao, Y. L. Hou, D. Ma, *J. Am. Chem. Soc.*, 2012, **134**, 15814-15821.
12 V. Schwartz, S. T. Oyama, *J. Mol. Catal A-Chem.*, 2000, **163**, 269-282.
13 V. Sundaramurthy, A. K. Dalai, J. Adjaye, *Appl. Catal. A*, 2006, **311**, 155-163.
14 L. Ramqvist, *Appl. Catal.*, 1971, **42**, 2113-2127.
15 W. Q. Zheng, T. P. Cotter, P. Kaghazchi, T. Jacob, B. Frank, K. Schlichte, W. Zhang, D. S. Su, F. Schuth, R. Schlogl, *J. Am. Chem. Soc.*, 2013, **135**, 3458-3464.
16 N. J. Lane, W. Barsoum, J. M. Rondinelli, *EPL*, 2013, **101**, 57004.
17 L. Volpe, M. Boudart, *J. Solid State Chem.*, 1985, **59**, 348.
18 E. Orhan, F. Tessier, R. Marchand, *Solid State Sci.*, 2002, **4**, 1071-1076.
19 Y. F. Shi, Y. Wan, R. L. Liu, B. Tu, D. Y. Zhao, *J. Am. Chem. Soc.*, 2007, **129**, 9522-9531.
20 H. M. Wang, X. H. Wang, M. H. Zhang, X. Y. Du, W. Li, K. Y. Tao, *Chem. Mater.*, 2007, **19**, 1801-1807.
21 Q. S. Gao, C. X. Zhang, S. H. Xie, W. M. Hua, Y. H. Zhang, N. Ren, H. L. Xu, Y. Tang, *Chem. Mater.*, 2009, **21**, 5560-5562.
22 Q. S. Gao, C. Giordano, M. Antonietti, *Small*, 2011, **7**, 3334-3340.
23 Q. S. Gao, S. N. Wang, Y. C. Ma, Y. Tang, C. Giordano, M. Antonietti, *Angew. Chem. Int. Ed.*, 2012, **51**, 961-965.
24 S. F. Zhuo, Y. Xu, W. W. Zhao, J. Zhang, B. Zhang, *Angew. Chem. Int. Ed.*, 2013, **52**, 8602-8606.
25 L. C. Yang, S. N. Wang, J. J. Mao, J. W. Deng, Q. S. Gao, Y. Tang, O. G. Schmidt, *Adv. Mater.*, 2013, **25**, 1180-1184.
26 L. Valade, R. Choukroun, P. Cassoux, F. Teyssandier, L. Poirier, M. Ducarroir, R. Feurer, P. Bonnefond, F. Maury, Eds., *Single-source precursors for the chemical vapor deposition of titanium and vanadium carbide and nitride*, Blackie Academic & Professional, Glasgow 1996.
27 S. Li, J. S. Lee, T. Hyeon, K. S. Suslick, *Appl. Catal. A*, 1999, **184**, 1-9.
28 D. Zeng, M. J. Hampden-Smith, *Chem. Mater.*, 1993, **5**, 681-689.
29 Q. S. Gao, C. X. Zhang, S. N. Wang, W. Shen, Y. H. Zhang, H. L. Xu, Y. Tang, *Chem. Commun.*, 2010, **46**, 6494-6496.
30 C. Giordano, C. Erpen, W. T. Yao, M. Antoniett, *Nano Lett.*, 2008, **8**, 4659-4663.
31 L. Liao, S. N. Wang, J. J. Xiao, X. J. Bian, Y. H. Zhang, M. D. Scanlon, X. L. Hu, Y. Tang, B. H. Liu, H. H. Girault, *Energy Environ. Sci.*, 2014, **7**, 387-392.
32 T. E. Mallouk, *Nat. Chem.*, 2013, **5**, 362-363.
33 N. Liu, L. C. Yang, S. N. Wang, Z. W. Zhong, S. N. He, X. Y. Yang, Q. S. Gao, Y. Tang, submitted.
34 C. G. Morales-Guio, L. Stern, X. L. Hu, *Chem. Soc. Rev.*, 2014, **43**, DOI: 10.1039/C1033CS60468C.
35 Q. S. Gao, S. N. Wang, H. C. Fang, J. W. Weng, Y. H. Zhang, J. J. Mao, Y. Tang, *J. Mater. Chem.*, 2012, **22**, 4709-4715.
36 P. Xiao, Y. Yan, X. M. Ge, Z. L. Liu, J. Y. Wang, X. Wang, *Appl. Catal. B*, 2014, **154-155**, 232-237.
37 C. Wan, Y. N. Regmi, B. M. Leonard, *Angew. Chem. Int. Ed.*, 2014, **53**, 6407-6410.
38 H. W. Huhosson, U. Jansson, B. Johansson, O. Eriksson, *Chem. Phys. Lett.*, 2001, **333**, 444-450.
39 W. F. Chen, S. Iyer, K. Sasaki, C. H. Wang, Y. M. Zhu, J. T. Muckerman, E. Fujita, *Energy Environ. Sci.*, 2013, **6**, 1818-1826.
40 D. J. Ham, R. Ganesan, J. S. Lee, *Int. J. Hydrogen Energ.*, 2008, **33**, 6865-6872.
41 A. T. Garcia-Esparza, D. Cha, Y. W. Ou, J. Kubota, K. Domen, K. Takanabe, *ChemSusChem*, 2013, **6**, 168-181.
42 N. S. Alhajri, H. Yoshida, D. H. Anjun, A. T. Garcia-Esparza, J. Kubota, K. Domen, K. Takanabe, *J. Mater. Chem. A*, 2013, **1**, 12606-12616.
43 X. L. Li, Y. D. Li, *Chem.-Eur. J.*, 2004, **10**, 433-439.
44 M. Pang, X. K. Wang, W. Xia, M. Muhler, C. H. Liang, *Ind. Eng. Chem. Res.*, 2013, **52**, 4564-4571.
45 C. Giordano, C. Erpen, W. T. Yao, B. Milke, M. Antonietti, *Chem. Mater.*, 2009, **21**, 5136-5144.
46 A. Garcia-Marquez, D. Portehault, C. Giordano, *J. Mater. Chem.*, 2011, **21**, 2136-2143.
47 A. Kraupner, M. Antonietti, R. Palkovits, K. Schlicht, C. Giordano, *J. Mater. Chem.*, 2010, **20**, 6019-6022.
48 A. Villa, S. Campisi, C. Giordano, K. Otte, L. Prati, *ACS Catal.*, 2012, **2**, 1377-1380.
49 W. T. Yao, P. Makowski, C. Giordano, F. Goettmann, *Chem.-Eur. J.*, 2009, **15**, 11999-12004.
50 X. J. Bian, M. D. Scanlon, S. N. Wang, L. Liao, Y. Tang, B. H. Liu, H. H. Girault, *Chem. Sci.*, 2013, **4**, 3432-3441.
51 S. H. Chai, V. Schwartz, J. Y. Howe, X. Q. Wang, M. Kidder, S. H. Overbury, S. Dai, D. E. Jiang, *Microporous Mesoporous Mater.*, 2013, **170**, 141-149.
52 N. Perret, X. D. Wang, L. Delannoy, C. Potvin, C. Louis, M. A. Keane, *J. Catal.*, 2012, **286**, 172-183.
53 C. H. Liang, P. L. Ying, C. Li, *Chem. Mater.*, 2002, **14**, 3148-3151.
54 B. Bokhonov, Y. Borisova, M. Korchagin, *Carbon*, 2004, **42**, 2067-2071.
55 S. M. de Lima, A. M. da Silva, L. O. O. da Costa, U. M. Graham, G. Jacobs, B. H. Davis, L. V. Mattos, F. B. Noronha, *J. Catal.*, 2009, **268**, 268-281.

56 Y. Zhao, K. Kamiya, K. Hashimoto, S. Nakanishi, *Angew. Chem. Int. Ed.*, 2013, **52**, 13638-13641.
57 T. Lunkenbein, D. Rosenthal, T. Otremba, F. Girgsdies, Z. H. Li, H. Sai, C. Bojer, G. Auffermann, U. Wiesner, J. Breu, *Angew. Chem. Int. Ed.*, 2012, **51**, 12892-12896.
58 R. Ganesan, J. S. Lee, *Angew. Chem. Int. Ed.*, 2005, **44**, 6557-6560.
59 Z. X. Yan, H. Meng, P. K. Shen, R. H. Wang, L. Wang, K. Y. Shi, H. G. Fu, *J. Mater. Chem.*, 2012, **22**, 5072-5079.
60 L. Borchardt, M. Oschatz, S. Graetz, M. R. Lohe, M. H. Ruemmeli, S. Kaskel, *Microporous Mesoporous Mater.*, 2014, **186**, 163-167.
61 J. S. J. Hargreaves, *Coordin. Chem. Rev.*, 2013, **257**, 2015-2031.
62 H. M. Wang, Z. J. Wu, J. Kong, Z. Q. Wang, M. H. Zhang, *J. Solid State Chem.*, 2012, **194**, 238-244.
63 P. Afanasiev, *Inorg. Chem.*, 2002, **41**, 5371-5319.
64 S. Chouzier, P. Afanasiev, M. Vrinat, T. Cseri, M. Roy-Auberger, *J. Solid State Chem.*, 2006, **179**, 3314.
65 S. Chouzier, M. Vrinat, T. Cseri, M. Roy-Auberger, P. Afanasiev, *Appl. Catal. A*, 2011, **400**, 82-90.
66 V. Molinari, C. Giordano, M. Antoniett, D. Esposito, *J. Am. Chem. Soc.*, 2014, **136**, 1758-1761.
67 M. Shalom, V. Molinari, D. Esposito, G. Clavel, D. Ressnig, C. Giordano, M. Antoniett, *Adv. Mater.*, 2014, **26**, 1272-1276.
68 Z. Schnepp, M. Thomas, S. Glatzel, K. Schlichte, R. Palkovits, C. Giordano, *J. Mater. Chem.*, 2011, **21**, 17760-17764.
69 X. H. Li, M. Antonietti, *Chem. Soc. Rev.*, 2013, **42**, 6593-6604.
70 R. C. V. McGee, S. K. Bej, L. T. Thompson, *Appl. Catal. A*, 2005, **284**, 139-146.
71 Y. G. Su, J. Y. Lang, L. P. Li, K. Guan, C. F. Du, L. M. Peng, D. Han, X. J. Wang, *J. Am. Chem. Soc.*, 2013, **135**, 11433-11436.
72 M. Y. Tsang, N. E. Pridmore, L. J. Gillie, Y. H. Chou, R. Brydson, R. E. Douthwaite, *Adv. Mater.*, 2012, **24**, 3406-3409.
73 M. Kerlau, O. Merdrignac-Conanec, M. Guilloux-Viry, A. Perrin, *Solid State Sci.*, 2004, **6**, 101-107.
74 H. Zhao, M. Lei, X. Chen, W. Tang, *J. Mater. Chem.*, 2006, **16**, 4407-4412.
75 J. Buha, I. Djerdj, M. Antonietti, M. Niederberger, *Chem. Mater.*, 2007, **19**, 3499-3505.
76 H. Schilling, A. Stork, E. Irran, H. Wolff, T. Bredow, R. Dronskowski, M. Lerch, *Angew. Chem. Int. Ed.*, 2007, **46**, 2931-2934.
77 Q. S. Gao, C. Giordano, M. Antonietti, *Angew. Chem. Int. Ed.*, 2012, **51**, 11740-11744.
78 M. R. Gao, J. Jiang, S. H. Yu, *Small*, 2012, **8**, 13-27.
79 J. J. Vittal, M. T. Ng, *Accounts Chem. Res.*, 2006, **39**, 869-877.
80 P. V. Vanitha, P. O'Brien, *J. Am. Chem. Soc.*, 2008, **130**, 17256-17266.
81 Y. J. Zhang, Y. P. Du, H. R. Xu, Q. B. Wang, *Cryst. Eng. Comm.*, 2010, **12**, 3658-3663.
82 Z. H. Zhang, W. S. Chin, J. J. Vittal, *J. Phys. Chem. B*, 2004, **108**, 18569-18574.
83 M. T. Ng, C. Boothroyd, J. J. Vittal, *Chem. Commun.*, 2005, 3820-3822.
84 S. K. Batabyal, L. Tian, N. Venkatram, W. Ji, J. J. Vittal, *J. Phys. Chem. C*, 2009, **113**, 15037-15042.
85 F. D. Wang, A. G. Dong, J. W. Sun, R. Tang, H. Yu, W. E. Buhro, *Inorg. Chem.*, 2006, **45**, 7511-7521.
86 J. W. Sun, W. E. Buhro, *Angew. Chem. Int. Ed.*, 2008, **47**, 3215-3218.
87 H. Yu, J. B. Li, R. A. Loomis, P. C. Gibbons, L. W. Wang, W. E. Buhro, *J. Am. Chem. Soc.*, 2003, **125**, 16168-16169.
88 A. C. Onicha, N. Petchsang, T. H. Kosel, M. Kuno, *ACS Nano*, 2012, **6**, 2833-2843.
89 M. Nath, A. Choudhury, A. Kundu, C. N. R. Rao, *Adv. Mater.*, 2003, **15**, 2098.
90 Z. A. Zhang, H. B. Yao, Y. X. Zhou, W. T. Yao, S. H. Yu, *Chem. Mater.*, 2008, **20**, 4749.
91 M. R. Gao, Q. Gao, J. Jiang, C. H. Cui, W. T. Yao, S. H. Yu, *Angew. Chem. Int. Ed.*, 2011, **50**, 4905-4908.
92 M. R. Gao, S. A. Liu, J. Jiang, C. H. Cui, W. T. Yao, S. H. Yu, *J. Mater. Chem.*, 2010, **20**, 9355-9361.
93 M. R. Gao, Y. F. Xu, J. Jiang, Y. R. Zheng, S. H. Yu, *J. Am. Chem. Soc.*, 2012, **134**, 2930-2933.
94 M. R. Gao, W. T. Yao, H. B. Yao, S. H. Yu, *J. Am. Chem. Soc.*, 2009, **131**, 7486-7487.
95 E. Antolini, T. Lopes, E. R. Gonzalez, *J. Alloy. Compd.*, 2008, **461**, 253-262.
96 H. Tong, Y. J. Zhu, L. X. Yang, L. Li, L. Zhang, *Angew. Chem. Int. Ed.*, 2006, **45**, 7739-7742.
97 S. N. Wang, Q. S. Gao, Y. H. Zhang, J. Gao, X. H. Sun, Y. Tang, *Chem.-Eur. J.*, 2011, **17**, 1465-1472.
98 C. F. Zhang, Z. Y. Wang, Z. P. Guo, X. W. Lou, *ACS Appl. Mater. Interfaces*, 2012, **4**, 3765-3768.
99 L. T. Kang, H. B. Fu, X. Q. Cao, Q. Shi, J. N. Yao, *J. Am. Chem. Soc.*, 2011, **133**, 1895-1901.
100 X. P. Sun, S. J. Dong, E. K. Wang, *J. Am. Chem. Soc.*, 2005, **127**, 13101-13103.
101 H. B. Yao, M. R. Gao, S. H. Yu, *Nanoscale*, 2010, **2**, 323-334.
102 Q. Liu, J. Q. Tian, W. Cui, P. Jiang, N. Y. Cheng, A. M. Asiri, X. P. Sun, *Angew. Chem. Int. Ed.*, 2014, **53**, 6710-6714.
103 J. Q. Tian, Q. Liu, A. M. Asiri, X. P. Sun, *J. Am. Chem. Soc.*, 2014, **136**, 7587-7590.
104 J. Q. Tian, Q. Liu, N. Y. Cheng, A. M. Asiri, X. P. Sun, *Angew. Chem. Int. Ed.*, 2014, **53**.
105 Z. C. Xing, Q. Liu, A. M. Asiri, X. P. Sun, *Adv. Mater.*, 2014, **26**, 5702-5707.